

QUANTIFYING ALTERNATIVE SPLICING FROM PAIRED-END RNA-SEQUENCING DATA

BY DAVID ROSSELL^{1,*} CAMILLE STEPHAN-OTTO ATTOLINI^{2,†}
MANUEL KROISS^{‡,§,3} AND ALMOND STÖCKER^{‡,3}

*University of Warwick**, *Institute for Research in Biomedicine of
Barcelona[†]*, *LMU Munich[‡]* and *TU Munich[§]*

RNA-sequencing has revolutionized biomedical research and, in particular, our ability to study gene alternative splicing. The problem has important implications for human health, as alternative splicing may be involved in malfunctions at the cellular level and multiple diseases. However, the high-dimensional nature of the data and the existence of experimental biases pose serious data analysis challenges. We find that the standard data summaries used to study alternative splicing are severely limited, as they ignore a substantial amount of valuable information. Current data analysis methods are based on such summaries and are hence suboptimal. Further, they have limited flexibility in accounting for technical biases. We propose novel data summaries and a Bayesian modeling framework that overcome these limitations and determine biases in a nonparametric, highly flexible manner. These summaries adapt naturally to the rapid improvements in sequencing technology. We provide efficient point estimates and uncertainty assessments. The approach allows to study alternative splicing patterns for individual samples and can also be the basis for downstream analyses. We found a severalfold improvement in estimation mean square error compared popular approaches in simulations, and substantially higher consistency between replicates in experimental data. Our findings indicate the need for adjusting the routine summarization and analysis of alternative splicing RNA-seq studies. We provide a software implementation in the R package *casper*.⁴

Received September 2012; revised May 2013.

¹Supported in part by Grants R01 CA158113-01 from the NIH (USA) and MTM2012-38337 from the Ministerio de Economía y Competitividad (Spain).

²Supported in part by AGAUR Beatriu de Pinós fellowship BP-B 00068 (Spain).

³Supported in part by a Bayerisches Arbeitsministerium foreign trainee fellowship (Germany).

Key words and phrases. Alternative splicing, RNA-Seq, Bayesian modeling, estimation.

This is an electronic reprint of the original article published by the [Institute of Mathematical Statistics](#) in *The Annals of Applied Statistics*, 2014, Vol. 8, No. 1, 309–330. This reprint differs from the original in pagination and typographic detail.

⁴<http://www.bioconductor.org/packages/release/bioc/html/casper.html>.

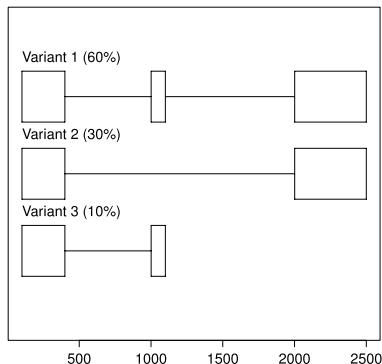


FIG. 1. *Three splice variants for a hypothetical gene and their relative abundances. Exon 1 is located at positions 101–400. Exon 2 at 1001–1100. Exon 3 at 2001–2500.*

1. Introduction. RNA-sequencing (RNA-seq) produces an overwhelming amount of genomic data in a single experiment, providing an unprecedented resolution to address biological problems. We focus on gene expression experiments where the goal is to study alternative splicing (AS), which we briefly introduce. AS is an important biological process by which cells are able to express several variants, also known as isoforms, of a single gene. Each splicing variant gives rise to a different protein with a unique structure that can perform different functions and respond to internal and environmental needs. AS is believed to contribute to the complexity of higher organisms, and is in fact particularly common in humans [Blencowe (2006)]. Additionally, it is known to be involved in multiple diseases such as cancer and malfunctions at the cellular level. Despite its importance, due to limitations in earlier technologies, most gene expression studies have ignored AS and focused on overall gene expression.

Consider the hypothetical example of a gene with three splice variants shown in Figure 1. The gene is encoded in the DNA in three exons, shown as boxes in Figure 1. When the gene is transcribed as messenger RNA (mRNA), it can give rise to three isoforms. Variant 1 is formed by all three exons, whereas variant 2 skips the second exon and variant 3 the third exon. Usually, multiple variants are expressed simultaneously at any given time. In our example, variant 1 makes up for 60% of the overall expression of the gene, variant 2 for 30% and variant 3 for 10%. In practice, these proportions are unknown and our goal is to estimate them as accurately as possible.

We focus on paired-end RNA-seq experiments, as they are the current standard and provide higher resolution for measuring isoform expression than competing technologies, for example, microarrays [Pepke, Wold and Mortazavi (2009)]. RNA-seq sequences tens or even hundreds of millions of mRNA fragments, which can then be aligned to a reference genome using

TABLE 1

Three paired-end RNA-seq fragments. Aligned chromosome and base pairs are indicated for both ends, allowing for gapped alignments. The exon path indicates the sequence of exons visited by each end. A typical experiment contains tens of millions of fragments

	Chromosome	Left read	Right read	Exon path
Fragment 1	chr1	110–185	200–274	{1}, {1}
Fragment 2	chr1	361–400; 1001–1035	2011–2085	{1, 2}, {3}
Fragment 3	chr1	301–375	1021–1095	{1}, {2}
...				

a variety of software, for example, TopHat [Trapnell, Pachter and Salzberg (2009)], SOAP [Li et al. (2009)] or BWA [Li and Durbin (2009)]. Throughout, we assume that the software can handle gapped alignments (we used TopHat in all our examples). Early RNA-seq studies used single-end sequencing, where only the left or right end of a fragment is sequenced. In contrast, paired-end RNA-seq sequences both fragment ends. Table 1 shows three hypothetical sequenced fragments corresponding to the gene in Figure 1. 75 base pairs (bp) were sequenced from each end. For instance, both ends of fragment 1 align to exon 1. As the three variants contain exon 1, in principle, this fragment could have been generated by any variant. For fragment 2 the left read aligned to exons 1 and 2 (i.e., it spanned the junction between both exons), and the right read to exon 3. Hence, fragment 2 can only have been generated from variant 1. Finally, fragment 3 visits exons 1 and 2 and, hence, it could have been generated either by variants 1 or 3. The example is simply meant to provide some intuition. In practice, most genes are substantially longer and have more complicated splicing patterns. Precise probability calculations are required to ensure that the conclusions are sound.

Ideally, one would want to sequence the whole variant, so that each fragment can be uniquely assigned to a variant. Unfortunately, current technologies sequence hundreds of base pairs, which are orders of magnitude shorter than typical variant lengths. Current statistical approaches are based on the observation that, while most sequenced fragments cannot be uniquely assigned to a variant, it is possible to make probability statements. For instance, fragment 3 in Table 1 may have originated either from variant 1 or 3, but the probability that each variant generates such a fragment is different. As we shall see below, this observation prompts a direct use of Bayes theorem.

In principle, one could formulate a probability model that uses the full data, that is, the exact base pairs covered by each fragment such as provided in Table 1, for example, Glaus, Honkela and Rattray (2012). However, our findings indicate that such strategies can be computationally prohibitive

and deliver no obvious improvement (Section 4). Further, data storage and transfer requirements impose a need for reducing the size of the data. Several authors proposed summarizing the data by counting the number of fragments either covering each exon or each exon junction [e.g., Xing et al. (2006), Mortazavi et al. (2008), Jiang and Wong (2009)]. In fact, large-scale genomic databases report precisely these summaries, for example, The Cancer Genome Atlas project.⁵ One can then pose a probability model that uses count data from a few categories as raw data, which greatly simplifies computation. While useful, this approach is seriously limited to considering pairwise junctions, which discards relevant information. For instance, suppose that a fragment visits exons 1, 2 and 3. Simply adding 1 to the count of fragments spanning exons 1–2 and 2–3 ignores the joint information that a single fragment visited 3 exons and decreases the confidence when inferring the variant that generated the fragment. Our results suggest that ignoring this information can result in a serious loss of precision. It is not uncommon that a fragment spans more than 2 exons. Holt and Jones (2008) found a substantial proportion of fragments bridging several exons in paired-end RNA-seq experiments. In the 2009 RGASP experimental data set (Section 4) 38.0% and 40.9% of fragments spanned ≥ 3 exons in replicate 1 and 2, respectively (we subdivided exons so that they are fully shared/not shared by all variants in a gene). In the 2012 ENCODE data set we found 64.7% and 65.2% in each replicate. The 2012 data had substantially longer reads and fragments, which illustrates the rapid advancements in technology. As sequencing evolves, these percentages are expected to increase further.

We propose novel data summaries that preserve most information relevant to alternative splicing, while maintaining the computational burden at a manageable level. We record the sequence of exons visited by each fragment end, which we refer to as *exon path*, and then count the number of fragments following each exon path. The left end of Fragment 2 in Table 1 visits exons 1 and 2 and the right end exon 3, which we denote as $\{1, 2\}, \{3\}$. Notice that a fragment following the path $\{1\}, \{2, 3\}$ visits the same exons, so one could be tempted to simply record $\{1, 2, 3\}$ in both cases. However, the probability of observing $\{1, 2\}, \{3\}$ for a given variant differs from $\{1\}, \{2, 3\}$ and, hence, combining the two paths would result in a potential loss of information. Table 2 contains hypothetical exon path counts for our example gene. We use these counts as the basic input for our probability model.

Paired-end RNA-seq is critical for AS studies. Intuitively, compared to single-end sequencing, it increases the probability of observing fragments that connect exon junctions. Lacroix et al. (2008) showed that, although neither protocol guarantees the existence of a unique solution, in practice,

⁵<http://cancergenome.nih.gov>.

paired-end (but not single-end) can provide asymptotically correct estimates for 99.7% of the human genes. In contrast, for single-end data the figure is 1.14%. Unfortunately, much of the current methodology has been designed with single-end data in mind. Xing et al. (2006) formulate the problem as that of traversing a directed acyclic graph and formulate a latent variable based approach to estimate splice variant expression. Jiang and Wong (2009) propose a similar approach within the Bayesian framework. Both approaches were designed for single-end RNA-seq data. Ameer et al. (2010) proposed strategies to detect splicing junctions, and Katz et al. (2010) and Wu et al. (2011) introduced models to estimate the percentage of isoforms skipping individual exons. However, these approaches do not estimate expression at the variant level.

Several authors propose strategies that use paired-ends. Mortazavi et al. (2008), Montgomery et al. (2010), Trapnell et al. (2010) and Salzman, Jiang and Wong (2011) model the number of fragments spanning exon junctions. These approaches focus on pairwise exon connections, ignoring valuable higher-order information, and have limitations in incorporating important technical biases. First, the sample preparation protocols usually induce an enrichment toward the 3' end of the transcript, that is, fragments are not uniformly distributed along the gene. Roberts et al. (2011a), Wu, Wang and Zhang (2011) or Glaus, Honkela and Rattray (2012) relax the uniformity assumption. Further, the fragment length distribution plays an important role in the probability calculations and needs to be estimated accurately. While the approaches above acknowledge this issue, they either use sequencing facility reports (i.e., they do not estimate the distribution from the data) or they impose strong parametric assumptions. Our examples illustrate that facility reports can be inaccurate and that parametric forms do not capture the observed asymmetries, heavy tails or multi-modalities. Further, all previous approaches assume that fragment start and length distributions are

TABLE 2
Exon path counts for hypothetical gene

Exon path	Count
{1}, {1}	2824
{2}, {2}	105
{3}, {3}	5042
{1}, {2}	27
{1}, {1, 2}	423
{1}, {3}	127
{2, 3}, {3}	394
{1, 2}, {3}	2
{1}, {2, 3}	13

constant across all genes. We provide empirical evidence that this assumption can be flawed and suggest a strategy to relax the assumption.

A concern with current genome annotations is that they may miss some splicing variants. Our approach can be combined with methods that predict new variants such as Cufflinks RABT module [Trapnell et al. (2010), Roberts et al. (2011b)], Scripture [Guttman et al. (2010)] or SpliceGrapher [Rogers et al. (2012)]. This option is implemented in our R package and illustrated in Section 4.3.

In summary, we propose a flexible framework to estimate alternative splicing from RNA-seq studies, by using novel data summaries and accounting for experimental biases. In Section 2 we formulate a probability model that goes beyond pairwise connections by considering exon paths. We model the read start and fragment size distributions nonparametrically and allow for separate estimation within subsets of genes with similar characteristics. Section 3 discusses model fitting and provides algorithms to obtain point estimates, asymptotic credibility intervals and posterior samples. We show some results in Section 4 and provide concluding remarks in Section 5.

2. Probability model. We formulate the model at the gene level and perform inference separately for each gene. In some cases, exons from different genes overlap with each other. When this occurs we group the overlapping genes and consider all their isoforms simultaneously. It is also possible that two variants share only a part of an exon. We subdivide such exons into the shared part and the part that is specific to each variant. For simplicity, from here on we refer to gene groups simply as genes and to subdivided exons simply as exons.

Consider a gene with E exons starting at base pairs s_1, \dots, s_E and ending at e_1, \dots, e_E . Denote the set of splicing variants under consideration by ν (assumed to be known) and its cardinality by $|\nu|$. Each variant is characterized by an increasing sequence of natural numbers i_1, i_2, \dots that indicates the exons contained therein.

2.1. Likelihood and prior. As discussed above, we formulate a model for exon paths. Let k be the number of exons visited by the left read, and k' be that for the right read (i.e., $k = k' = 1$ when both reads overlap a single exon). We denote an exon path by $\iota = (\iota_l, \iota_r)$, where $\iota_l = (i_j, \dots, i_{j+k})$ are the exons visited by the left-end and $\iota_r = (i_{j'}, \dots, i_{j'+k'})$ those by the right-end. Let \mathcal{P}^* be the set of all possible exon paths and \mathcal{P} be the subset of observed paths, that is, the paths followed by at least 1 sequenced fragment.

The observed data is a realization of the random variable $\mathbf{Y} = (Y_1, \dots, Y_N)$, where N is the number of paired-end reads and $Y_i \in \{1, \dots, \mathcal{P}^*\}$ indicates the exon path followed by read pair i . Formally, Y_i arises from a mixture of $|\nu|$ discrete probability distributions, each component corresponding to

a different splicing variant. The mixture weights $\boldsymbol{\pi} = (\pi_1, \dots, \pi_{|\nu|})$ give the proportion of reads generated by each variant, that is, its relative expression. That is,

$$P(Y_i = y_i | \boldsymbol{\pi}, \boldsymbol{\nu}) = \sum_{d=1}^{|\nu|} p_{y_i d} \pi_d,$$

where $p_{kd} = P(Y_i = k | \delta_i = d)$ is the probability of path k under variant d and δ_i is a latent variable indicating the variant that originated Y_i . Let S_i and L_i denote the relative start and length (resp.) of fragment i . The exon path Y_i is completely determined given S_i , L_i and the variant δ_i . Hence,

$$(1) \quad p_{kd} = \iint I(Y_i = k | S_i = s_i, L_i = l_i, \delta_i = d) dP_L(l_i | \delta_i) dP_S(s_i | \delta_i, L_i),$$

where P_L is the fragment distribution and P_S is the read start distribution conditional on L . As discussed in Section 2.2, by assuming that P_S and P_L are shared across sets of genes with similar characteristics, it is possible to estimate them with high precision. Hence, for practical purposes we can treat p_{kd} as known and pre-compute them before model fitting. Full derivations for p_{kd} are provided in Appendix A.

Assuming that each fragment is observed independently, the likelihood function can be written as

$$(2) \quad P(\mathbf{Y} | \boldsymbol{\pi}, \boldsymbol{\nu}) = \prod_{i=1}^N \sum_{d=1}^{|\nu|} p_{y_i d} \pi_d = \prod_{k=1}^{|\mathcal{P}|} \left(\sum_{d=1}^{|\nu|} p_{kd} \pi_d \right)^{x_k},$$

where $x_k = \sum_{i=1}^N I(y_i = k)$ is the number of reads following exon path k . Equation (2) is log-concave, which guarantees the existence of a single maximum. Log-concavity is given by (i) the log function being concave and monotone increasing, (ii) $\sum_{d=1}^{|\nu|} p_{kd} \pi_d$ being linear and therefore concave, and (iii) the fact that a composition $g \circ f$ where g is concave and monotone increasing and f is concave is again concave. To see (iii), notice that

$$\begin{aligned} g \circ f(t\mathbf{z}_1 + (1-t)\mathbf{z}_2) &\geq g(tf(\mathbf{z}_1) + (1-t)f(\mathbf{z}_2)) \\ &\geq tg \circ f(\mathbf{z}_1) + (1-t)g \circ f(\mathbf{z}_2), \end{aligned}$$

where the first inequality is given by g being increasing and f concave, and the second inequality is given by g being concave.

We complete the probability model with a Dirichlet prior on $\boldsymbol{\pi}$:

$$(3) \quad \boldsymbol{\pi} | \boldsymbol{\nu} \sim \text{Dir}(q_1, \dots, q_{|\nu|}).$$

In Section 4 we assess several choices for q_d . By default we set the fairly uninformative values $q_d = 2$, as these induce negligible bias and stabilize the

posterior mode by pooling it away from the boundaries 0 and 1. It is easy to see that (3) is log-concave when $q_d \geq 1$ for all d . Given that (2) is also log-concave, this choice of \mathbf{q} guarantees the posterior to be log-concave, and therefore the uniqueness of the posterior mode.

2.2. *Fragment length and read start distribution estimates.* Evaluating the exon path probabilities in (1) that appear in the likelihood (2) requires the fragment start distribution P_S and fragment length distribution P_L . Given that it is not possible to estimate (P_L, P_S) with precision for each individual gene, we assume they are shared across multiple genes (restricting fragments to be no longer than the variant they originated from). By default we assume that (P_L, P_S) are common across all genes, but we also studied posing separate distributions according to gene length. Supplementary Section 1 shows experimental evidence that, while P_L remains essentially constant, P_S can depend on gene length and the experimental setup. While this option is implemented in our R package, to allow a direct comparison with previous approaches here, we assumed a common (P_L, P_S) .

Denoting by T the length of variant δ_i (in bp), we let $P_L(l|\delta) = P_L(l|T) = P(L=l)\mathbf{I}(l \leq T)/P(l \leq T)$. That is, the conditional distribution of L given δ is simply a truncated version of the marginal distribution.

Further, we assume a common fragment start distribution relative to the variant length T . Conditional on L and T , P_S is truncated so that the fragment ends before the end of the variant. Specifically,

$$(4) \quad \begin{aligned} P_S(S \leq s | \delta_i, L = l) &= P\left(\frac{S}{T} \leq z | T, L = l\right) \\ &= \frac{\varphi(\min\{z, (T-l+1)/T\})}{\varphi((T-l+1)/T)}, \end{aligned}$$

where $z = s/T$ and $\varphi(z) = P(\frac{S}{T} \leq z)$ is the distribution of the relative read start $\frac{S}{T}$.

To estimate P_L note that the fragment length is unknown for fragments that span multiple exons, but it is known exactly when both ends fall in the same exon. Therefore, we select all such fragments and estimate P_L with the empirical probability mass function of the observed fragment lengths. In order to prevent short exons from inducing a selection bias, we only use exons that are substantially longer than the expected maximum fragment length (by default > 1000 bp).

Estimating the fragment start distribution P_S is more challenging, as we do not know the variant that generated each fragment and therefore its relative start position cannot be determined. We address this issue by selecting genes that have a single annotated variant, as, in principle, for these genes all fragments should have been generated by that variant. Of

course, the annotated genome does not contain all variants and, therefore, a proportion of the selected fragments may not have been generated by the assumed variant. However, the annotations are expected to contain most common variants (i.e., with highest expression) and, hence, most of the selected fragments should correspond to the annotated variant. Under this assumption, we can determine the exact start S_i and length L_i for all selected fragments. A difficulty in estimating the read start distribution is that the observed (S_i, L_i) pairs are truncated so that $S_i + L_i < T$, whereas we require the untruncated cumulative distribution function $\rho(\cdot)$ in (4). Fortunately, the truncation point for each (S_i, L_i) is known and, therefore, one can simply obtain a Kaplan–Meier estimate of $\rho(\cdot)$ [Kaplan and Meier (1958)]. We use the function `survfit` in the R `survival` package [Therneau and Lumley (2011)].

3. Model fitting. We provide algorithms to obtain a point estimate for $\boldsymbol{\pi}$, asymptotic credibility intervals and posterior samples.

Following a 0–1 loss, as a point estimate we report the posterior mode, which is obtained by maximizing the product of (2) and (3), subject to the constraint $\sum_{d=1}^{|\nu|} \pi_d = 1$. We note that maximum likelihood estimates are obtained by simply setting $q_d = 1$ in (3). This constrained optimization can be performed with many numerical optimization algorithms. Here we used the EM algorithm [Dempster, Laird and Rubin (1977)], as it is computationally efficient even when the number of variants $|\nu|$ is large. For a detailed derivation see Appendix B. As noted above, for $q_d > 1$ the log-posterior is concave and, therefore, the algorithm converges to the single maximum. The steps required for the algorithm are as follows:

1. Initialize $\pi_d^{(0)} = q_d / \sum_{d=1}^{|\nu|} q_d$.
2. At iteration j , update $\pi_d^{(j+1)} = q_d - 1 + \sum_{k=1}^{|\mathcal{P}|} x_k \frac{p_{kd} \pi_d^{(j)}}{\sum_{i=1}^{|\nu|} p_{ki} \pi_i^{(j)}}$.

Step 2 is repeated until the estimates stabilize. In our examples we required $|\pi_d^{(j+1)} - \pi_d^j| < 10^{-5}$ for all d . Notice that p_{kd} and x_k remain constant through all iterations and, hence, they need to be computed only once.

We characterize the posterior uncertainty asymptotically using a normal approximation in the re-parameterized space $\theta_d = \log(\pi_{d+1}/\pi_1)$, $d = 1, \dots, |\nu| - 1$ and the delta method [Casella and Berger (2001)]. Denote by $\boldsymbol{\mu}$ the posterior mode for $\boldsymbol{\theta} = (\theta_1, \dots, \theta_{|\nu|-1})$ and by S the Hessian of the log-posterior evaluated at $\boldsymbol{\theta} = \boldsymbol{\mu}$. Further, let $\pi(\boldsymbol{\theta})$ be the inverse transformation and $G(\boldsymbol{\theta})$ the matrix with (d, l) element $G_{dl} = \frac{\partial}{\partial \theta_l} \pi_d(\boldsymbol{\theta})$. Detailed expressions for S , $\pi(\boldsymbol{\theta})$ and $G(\boldsymbol{\theta})$ are provided in Appendix C. The posterior for $\boldsymbol{\theta}$ can be asymptotically approximated by $N(\boldsymbol{\mu}, \Sigma)$, where $\Sigma = S^{-1}$. Hence, the delta method approximates the posterior for $\boldsymbol{\pi}$ with $N(\pi(\boldsymbol{\mu}), G(\boldsymbol{\mu})' S G(\boldsymbol{\mu}))$.

The asymptotic approximation is also useful for the following independent proposal Metropolis–Hastings scheme. Initialize $\theta^{(0)} \sim T_3(\boldsymbol{\mu}, \Sigma)$ and notice that a prior $P_\pi(\boldsymbol{\pi})$ on $\boldsymbol{\pi}$ induces a prior $P_\theta(\boldsymbol{\theta}) = P_\pi(\boldsymbol{\pi}(\boldsymbol{\theta})) \times |G(\boldsymbol{\theta})|$ on $\boldsymbol{\theta}$, where $G(\boldsymbol{\theta})$ is as above. At iteration j , perform the following steps:

1. Propose $\boldsymbol{\theta}^* \sim T_3(\boldsymbol{\mu}, \Sigma)$ and let $\boldsymbol{\pi}^* = \boldsymbol{\pi}(\boldsymbol{\theta}^*)$.
2. Set $\boldsymbol{\theta}^{(j)} = \boldsymbol{\theta}^*$ with probability $\min\{1, \lambda\}$, where

$$(5) \quad \lambda = \frac{P(\mathbf{Y}|\boldsymbol{\pi}^*, \boldsymbol{\nu})P_\pi(\boldsymbol{\pi}^*)|G(\boldsymbol{\theta}^*)|}{P(\mathbf{Y}|\boldsymbol{\pi}^{(j-1)}, \boldsymbol{\nu})P_\pi(\boldsymbol{\pi}^{(j-1)})|G(\boldsymbol{\theta}^{(j-1)})|} \frac{T_3(\boldsymbol{\theta}^{(j-1)}; \boldsymbol{\mu}, \Sigma)}{T_3(\boldsymbol{\theta}^*; \boldsymbol{\mu}, \Sigma)}.$$

Otherwise, set $\boldsymbol{\theta}^{(j)} = \boldsymbol{\theta}^{(j-1)}$.

Posterior samples can be obtained by discarding some burn-in samples and repeating the process until practical convergence is achieved. By default we suggest 10,000 samples with a 1000 burn-in, as it provided sufficiently high numerical accuracy when comparing two independent chains (Supplementary Section 2).

4. Results. We assess the performance of our approach in simulations and two experimental data sets. We obtained the two human sample K562 replicates⁶ from the RGASP project (www.encodegenes.org/rgasp) and two ENCODE Project Consortium (2004) replicated samples obtained from A549 cells (accession number wgEncodeEH002625⁷). We compare our results with Cufflinks [Trapnell et al. (2012)], FluxCapacitor [Montgomery et al. (2010)] and BitSeq [Glaus, Honkela and Rattray (2012)]. Cufflinks is based on a probabilistic model akin to Casper, but uses exon and exon junction counts instead of full exon paths, assumes that fragment lengths are normally distributed and estimates the read start distribution in an iterative manner. FluxCapacitor is also based on exon and exon junction counts, but uses a method of moments type estimator. BitSeq uses a full Bayesian model at the base-pair resolution (i.e., data is not summarized as counts) and estimates the read start distribution with a two-step procedure.

Regarding sequence alignment, for Casper, Cufflinks and FluxCapacitor we used TopHat [Trapnell, Pachter and Salzberg (2009)] with the human genome hg19, using the default parameters and a 200 bp average insert size. BitSeq required aligning to the transcriptome with Bowtie [Langmead et al. (2009)].

⁶ftp://ftp.sanger.ac.uk/pub/encode/rgasp/RGASP1/inputdata/human_fastq/.

⁷genome.ucsc.edu/ENCODE.

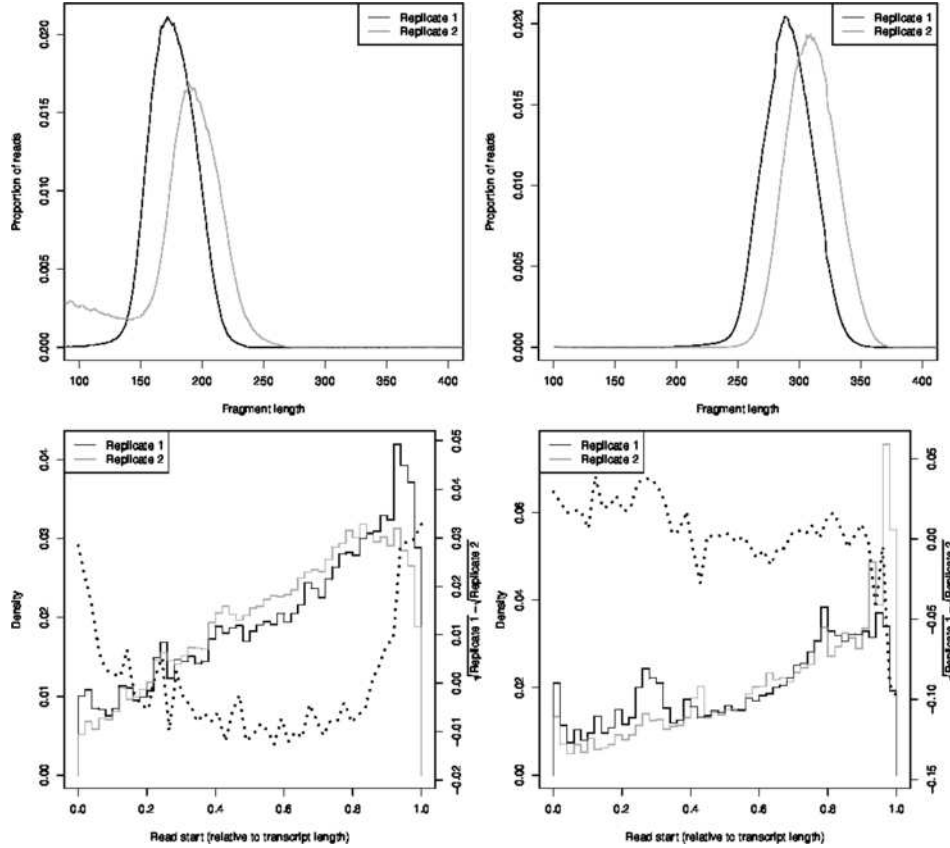


FIG. 2. Estimated fragment length (top) and start (bottom) distributions in K562 data (left) and A549 data (right). Black dotted line: difference in $\sqrt{P_S}$ between replicates (values in secondary y-axis).

4.1. *Simulation study.* We generated human genome-wide RNA-seq data, setting the simulations to resemble the K562 RGASP data in order to keep them as realistic as possible. Figure 2 (left) shows our estimates \hat{P}_S and \hat{P}_L . We set P_S and π for each gene with 2 or more variants to their estimates in the K562 data. For each gene we simulated a number of fragments equal to that observed in the K562 sample.

We considered a Casper-based and a Cufflinks-based simulation scenario. In the former we set π and P_L to the Casper estimates ($q_d = 2$). The second scenario was designed to favor Cufflinks by using its π estimates and setting P_L to its assumed Normal distribution (mean = 200, standard deviation = 20). We indicated the data-generating P_L to Cufflinks, whereas the remaining methods estimated it from the data. An important difference between scenarios is that Casper estimates with $q_d = 2$ are pooled away from

TABLE 3
Mean absolute and square errors, bias and variance for simulation study for Casper (top) and Cufflinks estimates (bottom)

	MAE	MSE	Bias sqrt	Variance
Casper-based simulations				
Casper ($q_d = 1$)	0.094	0.028	0.004	0.024
Casper ($q_d = 2$)	0.055	0.004	0.004	0.004
Cufflinks	0.141	0.050	0.028	0.022
FluxCapacitor	0.151	0.054	0.022	0.032
Cufflinks-based simulations				
Casper ($q_d = 1$)	0.100	0.055	0.021	0.034
Casper ($q_d = 2$)	0.111	0.035	0.032	0.003
Cufflinks	0.127	0.073	0.045	0.028
FluxCapacitor	0.138	0.078	0.036	0.042

the boundary, hence, π_d is never exactly 0 or 1, whereas the Cufflinks estimates were often in the boundary (Supplementary Figure 4). Genes with less than 10 reads per kilobase per million (RPKM) were excluded from all calculations to reduce biases due to low expression.

We estimated π from the simulated data using our approach with prior parameters $q_d = 1$ and $q_d = 2$, Cufflinks and FluxCapacitor. Table 3 reports the absolute and square errors ($|\pi_d - \hat{\pi}_d|$ and $(\pi_d - \hat{\pi}_d)^2$) averaged across all 18,909 isoforms and 100 simulated data sets for both simulation settings. We also report the average squared bias and variance. The Cufflinks and FluxCapacitor MAE are over 2.5 and 2.7 folds greater than that for Casper with $q_d = 2$ (1.5 and 1.6 for $q_d = 1$, resp.) in the Casper-based scenario. In the Cufflinks-based simulation the reductions were 1.14 and 1.24 fold (1.27 and 1.38 for $q_d = 1$). The improvements in MSE are even more pronounced, with an over 2 fold improvement for $q_d = 2$ even in the Cufflinks-based simulation. Casper also shows a marked improvement in bias for $q_d = 1$ and variance for $q_d = 2$. See Supplementary Figure 4 for corresponding plots.

Figure 3 (top) shows the MAE for each transcript as a function of RPKM, a measure of overall gene expression. Casper improves the estimates for essentially all RPKM values in both simulation settings. Figure 3 (bottom) assesses the MAE vs. the mean pairwise difference between variants in a gene (number of base pairs not shared). When variants in a gene share most exons this difference is small, that is, variants are harder to distinguish. Casper estimates are the most accurate at all similarity levels, with the MAE decreasing as variants become more differentiated. Interestingly, Cufflinks and FluxCapacitor show lower MAE as similarity increases from low to medium, but then MAE becomes higher and more variable in genes with medium-highly differentiated variants. These results illustrate the advantage

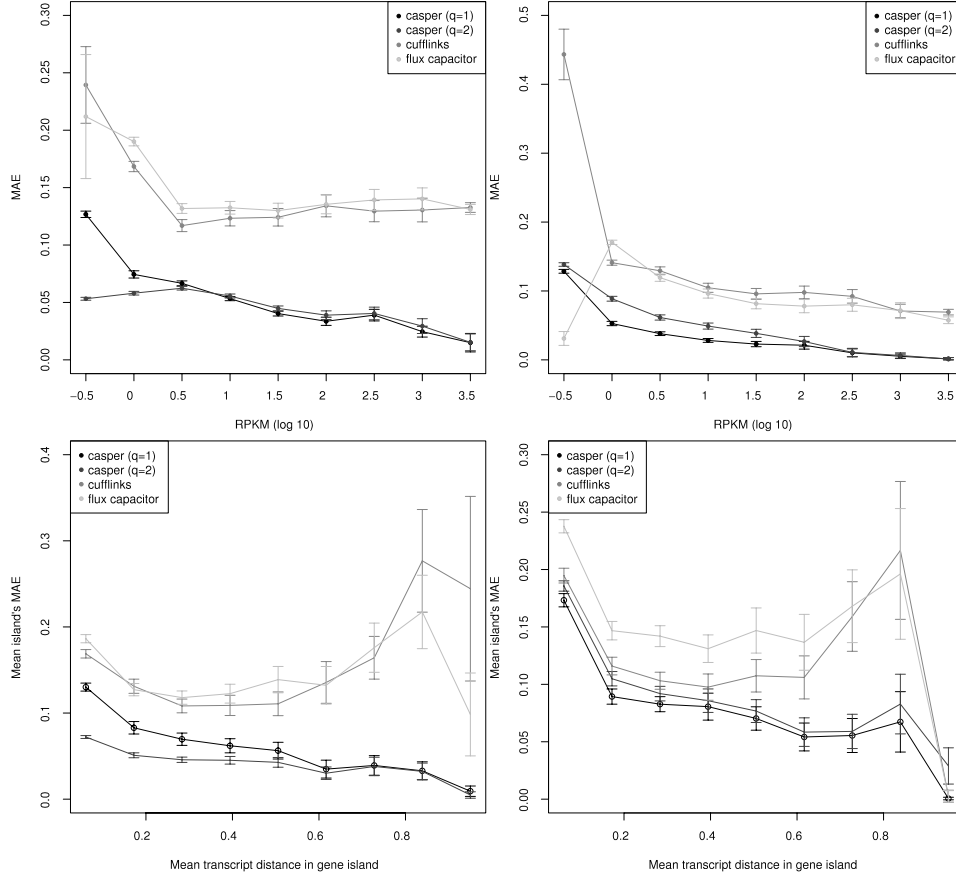


FIG. 3. *Simulation study. Mean absolute error vs. RPKM for Casper estimates (a) and Cufflink estimates (b) and the mean base pair difference between variants in a gene for Casper (c) and Cufflinks-based simulations (d).*

of using full exon paths, which provide more resolution in assigning reads to splicing variants.

Finally, we assessed the frequentist coverage probabilities for the asymptotic 95% credibility intervals (Section 3), finding that in 95.04% of the cases they contained the true value.

4.2. Experimental data from RGASP project. The two K562 replicates were sequenced in 2009 with Solexa sequencing. The read length was 75 bp and the mean fragment length indicated in the documentation is 200 bp for both replicates. Figure 2 (top, left) shows the estimated fragment length distributions. We observe that the mean length differs significantly from 200 bp and that there are important differences between replicates. Replicate 2 shows a heavy left tail that indicates a subset of fragments substantially

shorter than average. This distributional shape cannot be captured with the usual parametric distributions. Figure 2 (left, bottom) shows the relative start distribution. We observe more sequences located near the transcript end in replicate 1, that is, a higher 3' bias. The differences between replicates illustrate the need of flexibly modeling these distributions for each sample separately. In fact, we found that \hat{P}_S differed across genes with varying length (Supplementary Section 1 and Supplementary Figure 1), the 3' bias being stronger in genes shorter than 3 kilo-bases.

We estimated the expression of human splicing variants in the UCSC genome version hg19 for the two replicated samples separately. Figure 4 (left) and Table 4 compare the estimates obtained in the two samples. The Mean Absolute Difference (MAD) between replicates was 0.064 for Casper, 0.126 for Cufflinks (97% increase), 16.2 for FluxCapacitor (253% increase) and 8.5 for BitSeq (31% increase). Figure 4 shows a roughly linear correlation for Casper, Cufflinks and FluxCapacitor, the latter two frequently providing $\hat{\pi}_d = 0$ in one replicate and $\hat{\pi}_d = 1$ in the other. BitSeq avoids these boundaries but exhibits a strongly nonlinear association. In terms of computational time, all methods required roughly 10–20 min on 4 processors. Because BitSeq models the data at the base-pair resolution, it required substantially longer time to run on 12 cores.

These results suggest that Casper provides clear advantages even with earlier sequencing technologies.

4.3. Experimental data from ENCODE project. The two A549 replicated samples were sequenced in 2012 using Illumina HiSeq 2000. The read length was 101 bp and the average fragment length was roughly 300 bp (Figure 2, top right). These are substantially longer than the 2009 samples from Section 4.2, and reflect the improvement in sequencing technologies. Similar to Section 4.2, Figure 2 reveals important differences in the fragment length (top, right) and start (bottom, right) distributions between samples. See also Supplementary Section 1 and Supplementary Figure 2, where \hat{P}_S exhibits a stronger 3' bias for genes longer than 5 kilo-bases.

Figure 4 (left) and Table 4 compare the estimates obtained in the two replicates. Similar to the RGASP study (Section 4.2), Casper shows a roughly linear association and substantially higher consistency between replicates. The MAD between replicates was 0.057 for Casper, 9.0 for Cufflinks (58% increase), 12.7 for FluxCapacitor (223% increase) and 0.098 for BitSeq (72% increase). The computational time for Casper was comparable to that of Cufflinks, higher than FluxCapacitor and substantially lower than BitSeq. The findings show that the advantage of modeling exon path counts over pairwise exon connections remains pronounced as technology evolves to sequence longer fragments.

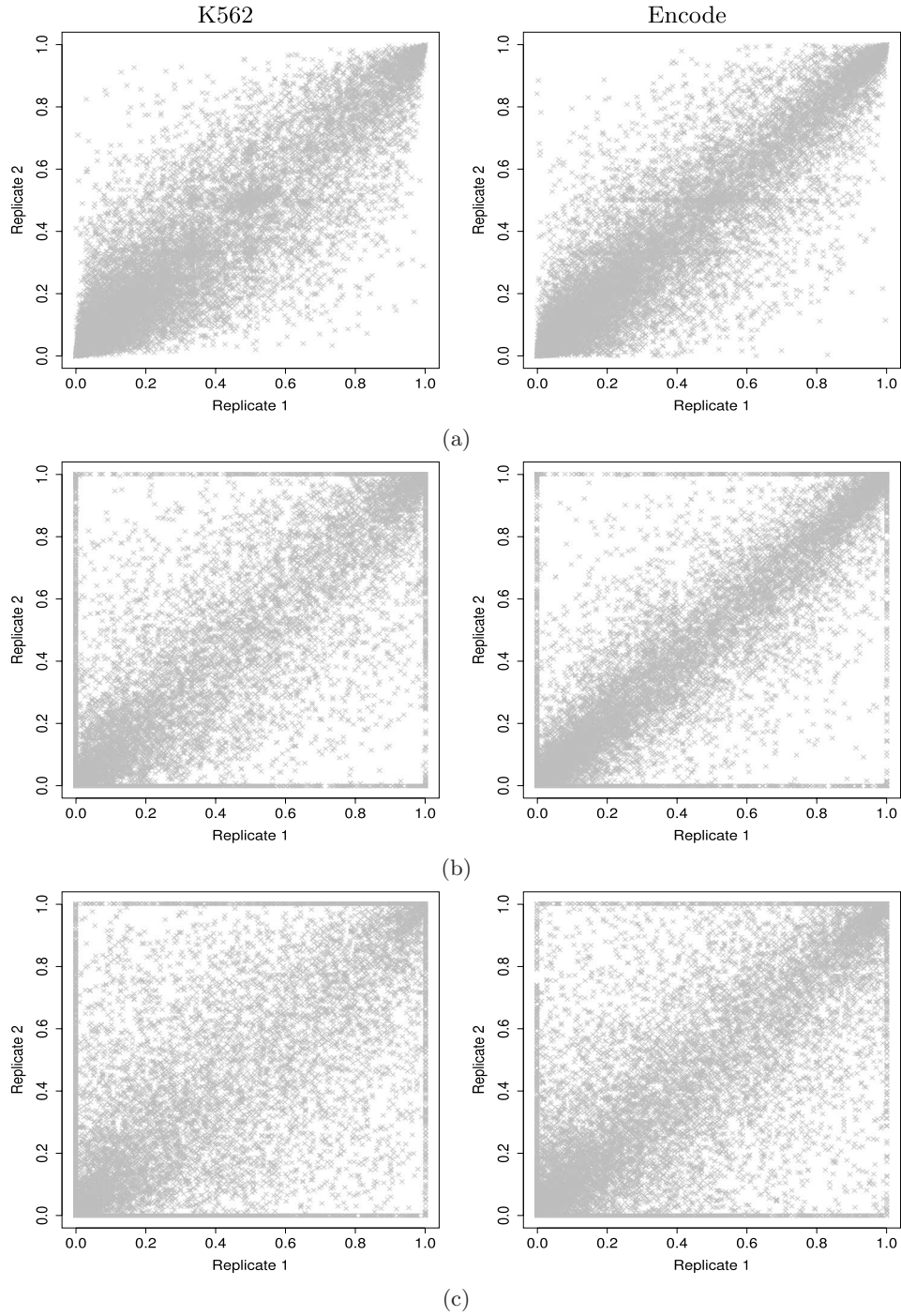


FIG. 4. Comparison of estimated isoform expression π_d between two replicates in K562 and ENCODE studies. (a) Casper with $q_d = 2$; (b) Cufflinks; (c) FluxCapacitor; (d) Bit-Seq.

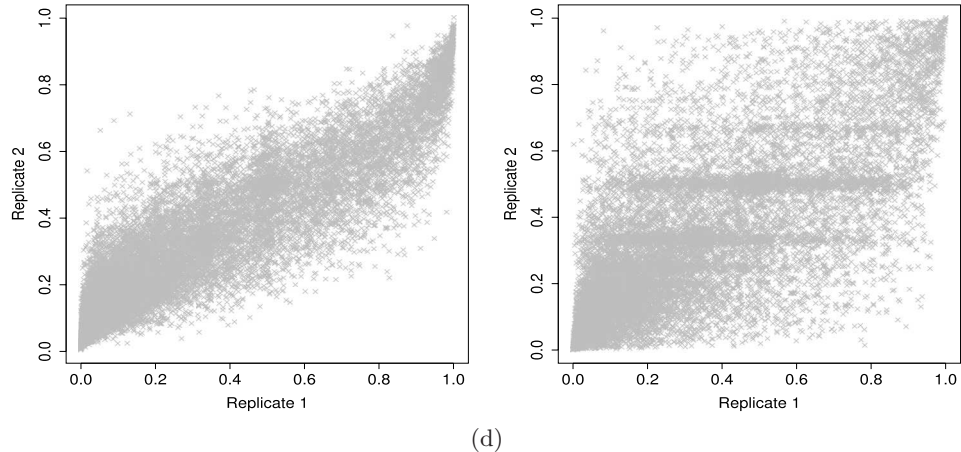


FIG. 4. (Continued).

We now consider the possibility that some expressed transcripts may not be present in the UCSC genome annotations. We used a Cufflinks RABT module to identify novel transcripts, and then run Casper to jointly estimate their expression with UCSC transcripts. Cufflinks-RABT found 12,512 gene islands with no new transcripts, 6229 with some new transcripts and 1527 completely new genes in sample 1. For sample 2 the figures were 11,912, 6983 and 1378 completely new genes. While new transcripts had negligible influence on genes with no new transcripts, in the remaining genes $\hat{\pi}_d$ decreased so that a proportion of the expression could be assigned to the new variants. For further details see Supplementary Section 4. These findings suggest that current genome annotations may miss a nonnegligible number of expressed variants. For a careful assessment we recommend following a strategy akin to ours here, that is, combining our approach with a *de novo* transcript discovery method.

TABLE 4
*K562 and Encode studies. Mean absolute difference (MAD) in $\hat{\pi}_d$ between replicates and CPU time on 2.8 GHz, 32 Gb OS X computer (+: 4 cores; *: 12 cores)*

	K562		Encode	
	MAD	CPU	MAD	CPU
Casper ⁺	6.4×10^{-2}	11.1 min	5.7×10^{-2}	2 h 11 min
Cufflinks ⁺	12.6×10^{-2}	21.4 min	9.0×10^{-2}	2h 13 min
Flux ⁺	16.2×10^{-2}	9.0 min	12.7×10^{-2}	1 h 17 min
BitSeq [*]	8.5×10^{-2}	1 day 13 h	9.8×10^{-2}	8 h 40 min

5. Discussion. We proposed a model to estimate the expression of a set of known alternatively spliced variants from RNA-seq data. The model improves upon previous proposals by using exon paths, which are more informative than single or pairwise exon counts, and by flexibly estimating the fragment start and length distributions. We provided computationally efficient algorithms for obtaining point estimates, asymptotic credibility intervals and posterior samples.

We found that a fairly uninformative prior with $q_d = 2$ improves precision relative to the typical $q_d = 1$ equivalent to maximum likelihood estimation. The advantages stem from the usual shrinkage argument: $q_d = 2$ pools the estimates away from the boundaries and reduces variance. Compared to competing approaches, we observed substantial MSE reductions in simulations and increased correlation between experimental replicates. In modern studies we found that roughly 2 sequences out of 3 visited > 2 exon regions distinguishing variants, suggesting that the current standard of reporting pairwise exon junctions adopted by most public databases is far from optimal. Reporting exon paths would allow researchers to estimate isoform expression at a much higher precision. Given that the methodology is implemented in the R package `casper`, we believe that it should be of great value to practitioners.

APPENDIX A: DERIVATION OF EXON PATH PROBABILITIES

Here we describe how to compute the probability p_{kd} of observing exon path k for any splicing variant d . Equivalently, we denote d by $\delta = (i_1, \dots, i_{|\delta|})$, where i_j indicates the j th exon within d . Consider variant δ after splicing, that is, after removing the introns. The new exon start positions are given by $s_1^* = 1$ and $s_{k+1}^* = s_k^* + e_{i_k} - s_{i_k} + 1$ for $k = 1, \dots, |\delta| - 1$. The end of exon k is $s_{k+1}^* - 1$. Denote by S the read start position, L the fragment length, r the read length, and let $T = s_{|\delta|}^* - 1$ be the transcript length of δ .

The goal is to compute $P(\boldsymbol{\iota}_l = (i_j, \dots, i_{j+k}), \boldsymbol{\iota}_r = (i_{j'}, \dots, i_{j'+k'}) | \delta)$. We note that both i_j, \dots, i_{j+k} and $i_{j'}, \dots, i_{j'+k'}$ must be consecutive exons under variant δ , otherwise the probability of the path is zero. The left read follows the exon path $\boldsymbol{\iota}_l = (i_j, \dots, i_{j+k})$ if and only if the read:

1. Starts in exon j , that is, $s_j^* \leq S \leq s_{j+1}^* - 1$.
2. Ends in exon $j + k$, that is, $s_{j+k}^* \leq S + r - 1 \leq s_{j+k+1}^* - 1$.

Similarly, the right read follows $\boldsymbol{\iota}_r = (i_{j'}, \dots, i_{j'+k'})$ if and only if $s_{j'}^* \leq S + L - r \leq s_{j'+1}^* - 1$ and $s_{j'+k'}^* \leq S + L - 1 \leq s_{j'+k'+1}^* - 1$. This implies that the desired probability can be written as $P(a_1 \leq S \leq b_1, a_2 \leq S + L \leq b_2 | \delta)$, where

$$a_1 = \max\{s_j^*, s_{j+k}^* - r + 1\},$$

$$(6) \quad \begin{aligned} b_1 &= \min\{s_{j+1}^* - 1, s_{j+k+1}^* - r\}, \\ a_2 &= \max\{s_{j'}^* + r, s_{j'+k'}^* + 1\}, \\ b_2 &= \min\{s_{j'+1}^* + r - 1, s_{j'+k'+1}^*\}. \end{aligned}$$

Assuming that the distribution of (S, L) depends on δ only through its transcript length T , we can write $P(a_1 \leq S \leq b_1, a_2 \leq S + L \leq b_2 | T) =$

$$(7) \quad \begin{aligned} &\sum_l P(a_1 \leq S \leq b_1, a_2 \leq S + L \leq b_2 | T, L = l) P(L = l | T) \\ &= \sum_l P(\max\{a_1, a_2 - L\} \leq S \leq \min\{b_1, b_2 - L\} | T, L = l) P(L = l | T). \end{aligned}$$

In order to evaluate (7), we need to estimate the fragment length distribution $P(L = l | T)$ and the distribution of the read start position S given L . We assume that $P(L | T) = P(L = l) \mathbf{I}(l \leq T) / P(L \leq T)$, that is, the conditional distribution of L given T is simply a truncated version of the marginal distribution. Further, notice that the fragment end must happen before the end of the transcript, that is, $S + L - 1 \leq T$ or, equivalently, the relative start position is truncated $S/T \leq S_T = (T - L + 1)/T$. The relative start distribution is therefore truncated, that is, $P(\frac{S}{T} \leq z | T, L = l) = \frac{\varphi(\min\{z, S_T\})}{\varphi(S_T)}$, where $\varphi(z) = P(\frac{S}{T} \leq z)$ is the distribution of the relative read start $\frac{S}{T}$.

Under these assumptions, the probability of observing the exon path $\boldsymbol{\iota}_l = (i_j, \dots, i_{j+k})$, $\boldsymbol{\iota}_r = (i_{j'}, \dots, i_{j'+k'})$ under variant δ is equal to

$$\begin{aligned} &\sum_l [(\varphi(\min\{b_1/T, (b_2 - l)/T, S_T\}) \\ &\quad - \varphi(\min\{\max\{(a_1 - 1)/T, (a_2 - l - 1)/T\}, S_T\})) / \varphi(S_T)]_+ P(L = l | T), \end{aligned}$$

where a_1 , b_1 , a_2 and b_2 are given in (6). Given that highly precise estimates of $P(L = l)$ and $\varphi(\cdot)$ are typically available, for computational simplicity we treat them as known and plug them into (8).

APPENDIX B: EM ALGORITHM DERIVATION

1. *E-step.*

Let $\delta_i \in \{1, \dots, |\nu|\}$ be latent variables indicating the variant that reads $i = 1, \dots, N$ come from. The augmented log-posterior is proportional to

$$(8) \quad \begin{aligned} l_0(\boldsymbol{\pi} | \mathbf{y}, \boldsymbol{\delta}) &= \log P(\boldsymbol{\pi} | \boldsymbol{\nu}) + \log P(\mathbf{y}, \boldsymbol{\delta} | \boldsymbol{\pi}) \\ &= \sum_{d=1}^{|\nu|} (q_d - 1) \log(\pi_d) + \sum_{i=1}^N \sum_{d=1}^{|\nu|} \mathbf{I}(\delta_i = d) [\log(p_{y_i d}) + \log(\pi_d)]. \end{aligned}$$

Considering δ_i as a random variable, the expected value of (8) given \mathbf{y} and $\boldsymbol{\pi} = \boldsymbol{\pi}^{(j)}$ is equal to

$$(9) \quad \begin{aligned} & E(l_0(\boldsymbol{\pi}'|\mathbf{y}, \boldsymbol{\delta})|\mathbf{y}, \boldsymbol{\pi}^{(j)}) \\ &= \sum_{d=1}^{|\nu|} (q_d - 1) \log(\pi_d) \\ &+ \sum_{i=1}^N \sum_{d=1}^{|\nu|} P(\delta_i = d|y_i, \boldsymbol{\pi}^{(j)}) (\log(p_{y_i,d}) + \log(\pi'_d)). \end{aligned}$$

2. *M-step.*

The goal is to maximize (9) with respect to $\boldsymbol{\pi}'$. Let $\gamma_{id} = P(\delta_i = d|y_i, \boldsymbol{\pi}^{(j)})$ and re-parameterize $\pi_{|\nu|} = 1 - \sum_{d=1}^{|\nu|-1} \pi_d$. Setting the partial derivatives with respect to π'_d to zero gives the system of equations

$$\frac{\pi'_d}{1 - \sum_{d=1}^{|\nu|-1} \pi'_d} = \frac{q_d - 1 + \sum_{i=1}^N \gamma_{id}}{q_{|\nu|} - 1 + \sum_{i=1}^N \gamma_{i|\nu|}},$$

which has the trivial solution $\pi'_d \propto q_d - 1 + \sum_{i=1}^N \gamma_{id}$. By plugging in $\gamma_{id} = p_{y_i,d} \pi_d^{(j)} / \sum_{d=1}^{|\nu|} p_{y_i,d} \pi_d^{(j)}$, we obtain

$$\pi'_d \propto q_d - 1 + \sum_{i=1}^N \frac{p_{y_i,d} \pi_d^{(j)}}{\sum_{d=1}^{|\nu|} p_{y_i,d} \pi_d^{(j)}}.$$

Finally, since $x_k = \sum_{i=1}^N \mathbb{I}(y_i = k)$, we can group all y_i 's taking the same value and find the maximum as

$$(10) \quad \pi'_d \propto q_d - 1 + \sum_{k=1}^{|\mathcal{P}|} x_k \frac{p_{kd} \pi_d^{(j)}}{\sum_{d=1}^{|\nu|} p_{kd} \pi_d^{(j)}},$$

re-normalizing $\boldsymbol{\pi}'$ so that $\sum_{d=1}^{|\nu|} \pi'_d = 1$.

APPENDIX C: ASYMPTOTIC POSTERIOR APPROXIMATION

Here we derive an asymptotic approximation to $P(\boldsymbol{\pi}|\boldsymbol{\nu}, \mathbf{Y})$, the posterior distribution of the splicing variants expression $\boldsymbol{\pi}$ conditional on a model $\boldsymbol{\nu}$ and the observed data \mathbf{Y} . Given that $\boldsymbol{\pi} = (\pi_1, \dots, \pi_{|\nu|}) \in [0, 1]^{|\nu|}$ with $\sum_{i=1}^{|\nu|} \pi_i = 1$, we re-parameterize to $\boldsymbol{\theta} = (\theta_1, \dots, \theta_{|\nu|-1}) \in \mathbb{R}^{|\nu|-1}$, where $\theta_d = \log(\frac{\pi_{d+1}}{\pi_1})$ for $d = 1, \dots, |\nu| - 1$. The goal is to approximate $P(\boldsymbol{\theta}|\boldsymbol{\nu}, \mathbf{Y}) \sim N(\boldsymbol{\mu}, \boldsymbol{\Sigma})$. For notational simplicity, in the remainder of the section we drop the conditioning on $\boldsymbol{\nu}$.

A prior $P_\pi(\boldsymbol{\pi})$ induces a prior $P_\theta(\boldsymbol{\theta}) = P_\pi(\boldsymbol{\pi}(\boldsymbol{\theta})) \times |G(\boldsymbol{\theta})|$ on $\boldsymbol{\theta}$, where $G(\boldsymbol{\theta})$ is the matrix with (d, l) element $G_{dl} = \frac{\partial}{\partial \theta_l} \pi_d(\boldsymbol{\theta})$ and inverse transform $\pi_1(\boldsymbol{\theta}) = (1 + \sum_{j=1}^{|\nu|-1} e^{\theta_j})^{-1}$, $\pi_d(\boldsymbol{\theta}) = \pi_1(\boldsymbol{\theta}) \exp\{\theta_{d-1}\}$ for $d > 1$.

Define $f(\boldsymbol{\theta}) = \log(P(\mathbf{Y}|\boldsymbol{\theta})) + \log(P_\theta(\boldsymbol{\theta}))$. Up to an additive constant, $f(\boldsymbol{\theta})$ is equal to the target log-posterior distribution of $\boldsymbol{\theta}$ given \mathbf{Y} . We center the approximating Normal at the posterior mode, that is, $\boldsymbol{\mu} = \operatorname{argmax}_{\boldsymbol{\theta} \in \mathbb{R}^{|\nu|-1}} f(\boldsymbol{\theta})$. We set $\Sigma = S^{-1}$, where S is the Hessian of $f(\boldsymbol{\theta})$ evaluated at $\boldsymbol{\theta} = \boldsymbol{\mu}$ with (l, m) element $S_{lm} = \frac{\partial^2}{\partial \theta_l \partial \theta_m} f(\boldsymbol{\theta})$. We approximate $\mu_d = \log(\frac{\pi_{d+1}^*}{\pi_d})$, where $\boldsymbol{\pi}^*$ is the posterior mode for $\boldsymbol{\pi}$ provided by the EM algorithm.

Under a $\boldsymbol{\pi} \sim \text{Dirichlet}(\mathbf{q})$ prior, simple algebra gives $\sigma_{lm} = \frac{\partial^2}{\partial \theta_l \partial \theta_m} f(\boldsymbol{\theta}) =$

$$(11) \quad \sum_{k=1}^{|\mathcal{P}|} x_k \frac{(\sum_{d=1}^{|\nu|} p_{kd} H_{dlm})(\sum_{d=1}^{|\nu|} p_{kd} \pi_d(\boldsymbol{\theta})) - (\sum_{d=1}^{|\nu|} p_{kd} G_{dl})(\sum_{d=1}^{|\nu|} p_{kd} G_{dm})}{(\sum_{d=1}^{|\nu|} p_{kd} \pi_d(\boldsymbol{\theta}))^2} + \sum_{d=1}^{|\nu|} (q_d - 1) \frac{H_{dlm} \pi_d(\boldsymbol{\theta}) - G_{dl} G_{dm}}{\pi_d(\boldsymbol{\theta})^2},$$

where $x_k = \sum_{i=1}^N \mathbf{I}(y_i = k)$ is the number of reads following exon path k , $p_{kd} = P(Y_i = k | \delta = d)$ is the probability of observing path k under variant d , the gradient for $\pi_d(\boldsymbol{\theta})$ is $G_{dl} = \frac{\partial}{\partial \theta_l} \pi_d(\boldsymbol{\theta})$ as before and the Hessian is $H_{dlm} = \frac{\partial^2}{\partial \theta_l \partial \theta_m} \pi_d(\boldsymbol{\theta})$.

We complete the derivation by providing expressions for G_{dl} and H_{dlm} . Let $s(\boldsymbol{\theta}) = 1 + \sum_{j=1}^{|\nu|-1} e^{\theta_j}$, then $G_{dl} =$

$$(12) \quad \begin{aligned} & \frac{-e^{\theta_l}}{s(\boldsymbol{\theta})^2} && \text{if } d = 1, \\ & \frac{-e^{\theta_{d-1} + \theta_l}}{s(\boldsymbol{\theta})^2} + \mathbf{I}(l = d - 1) \frac{e^{\theta_l}}{s(\boldsymbol{\theta})} && \text{if } d \geq 2 \end{aligned}$$

and $H_{dlm} =$

$$(13) \quad \begin{aligned} & \frac{2e^{\theta_l + \theta_m}}{s(\boldsymbol{\theta})^3} - \mathbf{I}(l = m) \frac{e^{\theta_l}}{s(\boldsymbol{\theta})^2} && \text{if } d = 1, \\ & \frac{2e^{\theta_{d-1} + \theta_l + \theta_m}}{s(\boldsymbol{\theta})^3} - \mathbf{I}(l = d - 1) \frac{e^{\theta_l + \theta_m}}{s(\boldsymbol{\theta})} && \text{if } d \geq 2, m \neq l, m \neq d - 1, \\ & \frac{-2e^{2\theta_m}}{s(\boldsymbol{\theta})^2} + \frac{2e^{3\theta_m}}{s(\boldsymbol{\theta})^3} + \frac{e^{\theta_m}}{s(\boldsymbol{\theta})} - \frac{2e^{2\theta_m}}{s(\boldsymbol{\theta})^2} && \text{if } d \geq 2, m = l, m = d - 1, \\ & \frac{-e^{\theta_{d-1} + \theta_l}}{s(\boldsymbol{\theta})^2} + \frac{2e^{\theta_{d-1} + \theta_l + \theta_m}}{s(\boldsymbol{\theta})^3} && \text{otherwise.} \end{aligned}$$

Acknowledgments. D. Rossell and C. Stephan-Otto Attolini contributed equally to this work. The authors wish to thank Modesto Orozco for useful discussions.

SUPPLEMENTARY MATERIAL

Supplementary results (DOI: [10.1214/13-AOAS687SUPP](https://doi.org/10.1214/13-AOAS687SUPP); .pdf). In Rossell et al. (2014) we assess the dependence of fragment start and length distributions on gene length, show additional simulation results, assess MCMC convergence and apply the approach to transcripts found *de novo*.

REFERENCES

- AMEUR, A., WETTERBOM, A., FEUK, L. and GYLLENSTEN, U. (2010). Global and unbiased detection of splice junctions from RNA-seq data. *Genome Biol.* **11** R34.
- BLENCOWE, B. J. (2006). Alternative splicing: New insights from global analyses. *Cell* **126** 37–47.
- CASELLA, G. and BERGER, R. L. (2001). *Statistical Inference*, 2nd ed. Duxbury, N. Scituate.
- DEMPSTER, A. P., LAIRD, N. M. and RUBIN, D. B. (1977). Maximum likelihood from incomplete data via the EM algorithm. *J. R. Stat. Soc. Ser. B Stat. Methodol.* **39** 1–38. [MR0501537](#)
- ENCODE Project Consortium (2004). The ENCODE (ENCyclopedia Of DNA Elements) Project. *Science* **306** 636–640.
- GLAUS, P., HONKELA, A. and RATTRAY, M. (2012). Identifying differentially expressed transcripts from RNA-seq data with biological variation. *Bioinformatics* **28** 1721–1728.
- GUTTMAN, M., GARBER, M., LEVIN, J. Z., DONAGHEY, J., ROBINSON, J., ADICONIS, X., FAN, L., KOZIOL, M. J., GNIRKE, A., NUSBAUM, C., RINN, J. L., LANDER, E. S. and REGEV, A. (2010). Ab initio reconstruction of cell type-specific transcriptomes in mouse reveals the conserved multi-exonic structure of lincRNAs. *Nature Biotechnology* **28** 503–510.
- HOLT, R. A. and JONES, S. J. M. (2008). The new paradigm of flow cell sequencing. *Genome Research* **18** 839–846.
- JIANG, H. and WONG, W. H. (2009). Statistical inferences for isoform expression in RNA-Seq. *Bioinformatics* **25** 1026–1032.
- KAPLAN, E. L. and MEIER, P. (1958). Nonparametric estimation from incomplete observations. *J. Amer. Statist. Assoc.* **53** 457–481. [MR0093867](#)
- KATZ, Y., WANG, E. T., AIROLDI, E. M. and BURGE, C. B. (2010). Analysis and design of RNA sequencing experiments for identifying isoform regulation. *Nat. Methods* **7** 1009–1015.
- LACROIX, V., SAMMETH, M., GUIGO, R. and BERGERON, A. (2008). Exact Transcriptome Reconstruction from Short Sequence Reads. In *Proceedings of the 8th International Workshop on Algorithms in Bioinformatics*. 50–63. Springer, Berlin.
- LANGMEAD, B., TRAPNELL, C., POP, M. and SALZBERG, S. L. (2009). Ultrafast and memory-efficient alignment of short DNA sequences to the human genome. *Genome Biol.* **10** R25.
- LI, H. and DURBIN, R. (2009). Fast and accurate short read alignment with Burrows–Wheeler transform. *Bioinformatics* **25** 1754–1760.

- LI, R., YU, C., LI, Y., LAM, T. W., YIU, S. M., KRISTIANSEN, K. and WANG, J. (2009). SOAP2: An improved ultrafast tool for short read alignment. *Bioinformatics* **25** 1966–1967.
- MONTGOMERY, S. B., SAMMETH, M., GUTIERREZ-ARCELUS, M., LACH, R. P., INGLE, C., NISBETT, J., GUIGO, R. and DERMITZAKIS, E. T. (2010). Transcriptome genetics using second generation sequencing in a Caucasian population. *Nature* **464** 773–777.
- MORTAZAVI, A., WILLIAMS, B. A., MCCUE, K., SCHAEFFER, L. and B., W. (2008). Mapping and quantifying mammalian transcriptomes by RNA-Seq. *Nature Methods* **5** 621–628.
- PEPKE, S., WOLD, B. and MORTAZAVI, A. (2009). Computation for ChIP-seq and RNA-seq studies. *Nat. Methods* **6** S22–S32.
- ROBERTS, A., TRAPNELL, C., DONAGHEY, J., RINN, J. L. and PACHTER, L. (2011a). Improving RNA-Seq expression estimates by correcting for fragment bias. *Genome Biol.* **12** R22.
- ROBERTS, A., PIMENTEL, H., TRAPNELL, C. and PACHTER, L. (2011b). Identification of novel transcripts in annotated genomes using RNA-Seq. *Bioinformatics* **27** 2325–2329.
- ROGERS, M. F., THOMAS, J., REDDY, A. S. and BEN-HUR, A. (2012). SpliceGrapher: Detecting patterns of alternative splicing from RNA-Seq data in the context of gene models and EST data. *Genome Biol.* **13** R4.
- ROSSELL, D., STEPHAN-OTTO ATTOLINI, C., KROISS, M. and STÖCKER, A. (2014). Supplement to “Quantifying alternative splicing from paired-end RNA-sequencing data.” DOI:[10.1214/13-AOAS687SUPP](https://doi.org/10.1214/13-AOAS687SUPP).
- SALZMAN, J., JIANG, H. and WONG, W. H. (2011). Statistical modeling of RNA-Seq data. *Statist. Sci.* **26** 62–83. [MR2849910](https://doi.org/10.1214/11-SS123)
- THERNEAU, T. and LUMLEY, T. (2011). Survival: Survival analysis, including penalised likelihood. R package version 2.36-10.
- TRAPNELL, C., PACHTER, L. and SALZBERG, S. L. (2009). TopHat: Discovering splice junctions with RNA-Seq. *Bioinformatics* **25** 1105–1111.
- TRAPNELL, C., WILLIAMS, B. A., PERTEA, G., MORTAZAVI, A., KWAN, G., VAN BAREN, M. J., SALZBERG, S. L., WOLD, B. J. and PACHTER, L. (2010). Transcript assembly and quantification by RNA-Seq reveals unannotated transcripts and isoform switching during cell differentiation. *Nat. Biotechnol.* **28** 511–515.
- TRAPNELL, C., ROBERTS, A., GOFF, L., PERTEA, G., KIM, D., KELLEY, D. R., PIMENTEL, H., SALZBERG, S. L., RINN, J. L. and PACHTER, L. (2012). Differential gene and transcript expression analysis of RNA-seq experiments with TopHat and Cufflinks. *Nature Protocols* **7** 562–578.
- WU, Z., WANG, X. and ZHANG, X. (2011). Using non-uniform read distribution models to improve isoform expression inference in RNA-Seq. *Bioinformatics* **27** 502–508.
- WU, J., AKERMAN, M., SUN, S., MCCOMBIE, W. R., KRAINER, A. R. and ZHANG, M. Q. (2011). SpliceTrap: A method to quantify alternative splicing under single cellular conditions. *Bioinformatics* **27** 3010–3016.
- XING, Y., YU, T., WU, Y. N., ROY, M., KIM, J. and LEE, C. (2006). An expectation–maximization algorithm for probabilistic reconstructions of full-length isoforms from splice graphs. *Nucleic. Acids Res.* **34** 3150–3160.

D. ROSSELL
DEPARTMENT OF STATISTICS
UNIVERSITY OF WARWICK
GIBBEL HILL RD.
COVENTRY CV4 7AL
UNITED KINGDOM
E-MAIL: D.Rossell@warwick.ac.uk

C. STEPHAN-OTTO ATTOLINI
INSTITUTE FOR RESEARCH IN BIOMEDICINE
OF BARCELONA
BALDIRI REIXAC 10
BARCELONA 08028
SPAIN
E-MAIL: camille.stephan@irbbarcelona.org

M. KROISS
LMU MUNICH
GESCHWISTER-SCHOLL-PLATZ 1
MÜNCHEN 089 2180-0
GERMANY
E-MAIL: kroissm@in.tum.de

A. STÖCKER
TU MUNICH
GESCHWISTER-SCHOLL-PLATZ 1
MÜNCHEN 089 2180-0
GERMANY
E-MAIL: al.st@web.de

CORRIGENDUM
QUANTIFYING ALTERNATIVE SPLICING FROM
PAIRED-END RNA-SEQ DATA

BY DAVID ROSSELL*, CAMILLE STEPHAN-OTTO ATTOLINI†,
MANUEL KROISS‡,§ AND ALMOND STÖCKER‡

*University of Warwick**, *Institute for Research in Biomedicine of*
Barcelona†, *LMU Munich‡* and *TU Munich§*

In Figure 4(d) of Rossell et al. (2014) (Section 4.3), we followed the standard pipeline for BitSeq and used the bowtie aligner (versus Tophat for the other methods, casper, Cufflinks and BitSeq). The BitSeq authors noted that we used the bowtie1 version, which gave very low mapping rates (<2% aligned reads in both samples). Figure 1 below uses bowtie2, which gives mapping rates >70% (the MAD between replicates also drops, from 0.098 to 0.062). We thank the Bitseq authors for alerting us to bowtie2.

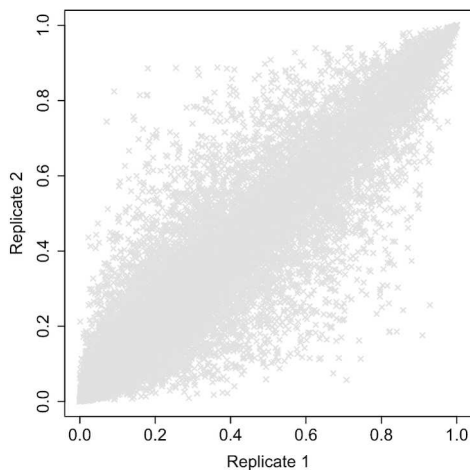


FIG. 1. *Corrected Figure 4d, right panel.*

Received March 2015; revised June 2015.

This is an electronic reprint of the original article published by the Institute of Mathematical Statistics in *The Annals of Applied Statistics*, 2015, Vol. 9, No. 3, 1706–1707. This reprint differs from the original in pagination and typographic detail.

REFERENCE

ROSSELL, D., STEPHAN-OTTO ATTOLINI, C., KROISS, M. and STÖCKER, A. (2014). Quantifying alternative splicing from paired-end RNA-sequencing data. *Ann. Appl. Stat.* **8** 309–330. [MR3191992](#)

D. ROSSELL
DEPARTMENT OF STATISTICS
UNIVERSITY OF WARWICK
GIBBEL HILL RD.
COVENTRY CV4 7AL
UNITED KINGDOM
E-MAIL: D.Rossell@warwick.ac.uk

M. KROISS
LMU MUNICH
GESCHWISTER-SCHOLL-PLATZ 1
MÜNCHEN 089 2180-0
GERMANY
E-MAIL: kroissm@in.tum.de

C. STEPHAN-OTTO ATTOLINI
INSTITUTE FOR RESEARCH IN BIOMEDICINE
OF BARCELONA
BALDIRI REIXAC 10
BARCELONA 08028
SPAIN
E-MAIL: camille.stephan@irbbarcelona.org

A. STÖCKER
TU MUNICH
GESCHWISTER-SCHOLL-PLATZ 1
MÜNCHEN 089 2180-0
GERMANY
E-MAIL: al.st@web.de